Shap. Mem. Superelasticity (2016) 2:228–234
DOI 10.1007/s40830-016-0069-9

Microstructure and Mechanical Properties in B-Doped Fe-31.9Ni-9.6Co-4.7Ti Alloys

Doyup Lee[1] · Toshihiro Omori[1] · Ryosuke Kainuma[1]

Published online: 22 April 2016

Abstract Effects of the addition of boron on grain boundary precipitation, martensitic transformation temperatures, and mechanical properties were investigated for Fe-31.9Ni-9.6Co-4.7Ti alloy sheets. Grain boundary precipitation of the η-Ni3Ti phase with the D024 structure, which significantly deteriorates the mechanical properties, is effectively suppressed by the addition of a small amount of B. Both the transformation temperature and the thermal hysteresis slightly increase with increasing B composition. Tensile fracture elongation is improved to be about 1.3 % by addition of 0.05 % B, but no superelastic property was detected in the cyclic stress–strain curve. The features in the mechanical properties are discussed with the texture properties in the sheet specimen.

Keywords Mechanical behavior · Thermoleastic · Fe–Ni–Co–Ti · Grain boundary precipitation

Introduction

Ni–Ti-based shape memory alloys (SMAs) exhibiting moderate ductility and an excellent superelastic (SE) strain of over 7 % are used in many products such as cellar phone antennae, spectacle frames, medical guidewires, stents, and so on. However, since the cold-workability of Ni–Ti-based polycrystalline SMAs is insufficient and its material and fabrication costs are relatively high, its applications to wider fields are impeded [1].

Up to now, some ferrous polycrystalline alloys, such as Fe–Mn–Si [2, 3], Fe–Ni–C [4], and Fe–Ni–Co–Ti [5–8], have been developed as "ferrous SMAs" because their better workability and lower cost are commercially more attractive than those of Ni–Ti-based SMAs. One of the most serious drawbacks of these ferrous SMAs in practical use has been their poor superelasticity due to non-thermoelastic martensitic transformation with a large thermal transformation hysteresis, except in the case of noble ferrous alloys such as Fe–Pt and Fe–Pd [1]. In 1984, Maki et al. first observed a thermoelastic microstructural behavior at 173 K in γ/α' (bct) transformation of a Fe-31.9Ni-9.6Co-4.7Ti (at. %) [Fe-33Ni-10Co-4Ti (mass %)] alloy by the precipitation of a metastable γ'-$(Ni,Fe,Co)_3Ti$ phase with an $L1_2$ structure [6]. According to Maki, the following four factors are necessary to obtain thermoelastic martensitic transformation in ferrous SMAs [1]: (1) high hardness of the matrix, (2) low *M*s temperature, (3) low transformation volume change, and (4) large tetragonality of the martensite. Using these guideline, Kokorin et al. have confirmed an SE strain of approximately 0.7 % in a bending test at 240 K for Fe-28.9Ni-18.2Co-8.3Ti [Fe-30Ni-19Co-7Ti (mass %)] alloy [7]. However, brittleness due to grain boundary precipitation of an η-Ni_3Ti phase with a $D0_{24}$ structure restricts the increase of ductility and SE strain, meaning that this alloy is of no practical use.

Recently, a number of research groups have reported three different kinds of ferrous SMAs, Fe–Ni–Co–Al-based alloys (from fcc to bct) [9–20], Fe–Mn–Ga alloy (from $L2_1$ to $D0_{22}$) [21, 22], and Fe–Mn–Al–Ni alloy (from bcc to nano-twinned fcc) [23–28], showing thermoelastic transformation. In case of the Fe–Ni–Co–Al-based and Fe–Mn–Al–Ni alloys, strengthening of the parent phase resulting

✉ Doyup Lee
doyup.lee.q3@dc.tohoku.ac.jp

[1] Department of Materials Science, Graduate School of Engineering, Tohoku University, 6-6-02 Aobayama, Sendai, Miyagi 980-8579, Japan

from fine and coherent precipitates of the γ' phase with the $L1_2$ structure and the β phase with the *B2* structure by aging heat treatment are important to realize thermoelastic transformation and SE properties, respectively. Especially, in Fe–Ni–Co–Al–Ta–B alloy, the polycrystalline sheet specimens strengthened by the γ'-$(Ni, Fe, Co)_3(Al, Ta)$ phase and strongly textured by thermomechanical treatment exhibit large maximum SE strain of about 13.5 %, which is approximately twice that of Ni–Ti alloy [9]. Furthermore, noted SE strains of more than 4 % were also confirmed in not only Fe–Ni–Co–Al–Ta single-crystal alloys [10–14] but also in Fe–Ni–Co–Al–Nb-based polycrystalline [16] and Fe–Ni–Co–Al–Ti-based [17–19] single-crystal alloys, where Ta is substituted by Nb and Ti, well known as γ' stabilizer elements in Ni-based alloys [29]. The addition of B in Fe–Ni–Co–Al-based single-crystal alloys is unnecessary because being a nucleation site of grain boundary precipitation, it does not contain grain boundaries, whereas in the case of polycrystalline alloys [9, 16, 18, 20], the addition of a small amount of boron plays an important role in the drastic suppression of the undesirable β-NiAl B2 phase appearing on grain boundaries. However, improvement of ductility and SE strain is not satisfied only by the addition of boron. As mentioned above, in the case of polycrystalline alloy, the SE strain can be obtained only in strongly textured sheet specimens by suitable thermomechanical treatment. This means that control of the characteristics of the grain boundary, which decreases the fraction of high-angle boundaries, is also important for further suppression of grain boundary precipitation.

In this study, the effects of the addition of boron and thermomechanical treatment on the grain boundary precipitation of the η-Ni_3Ti phase, martensitic transformation temperatures, and mechanical properties were investigated for the Fe-31.9Ni-9.6Co-4.7Ti (at.%) polycrystalline alloy with relatively low Co and Ti compositions, which has been proposed by T. Maki et al. [6].

Experimental Procedures

Fe-31.9Ni-9.6Co-4.7Ti-(0, 0.02, 0.05, and 0.08)B alloys (at%) (hereafter notated as 0B, 0.02B, 0.05B, and 0.08B, respectively) were selected for the present study. Cylindroid ingots of 20 mm in diameter were prepared by induction melting under an argon atmosphere. The ingots were hot-rolled at 1473 K to a thickness of 14 mm, followed by ice water quenching. And then the top and bottom surfaces were polished to eliminate scale. The specimens with a thickness of 13.5 mm were cold-rolled to thickness of a 0.2 mm without intermediate annealing, where the cold-rolling reduction was 98.5 %. This rolling procedure was repeated about 105 times. The sheets were solution-treated at 1473 K for 3 h to obtain a γ single-phase structure and then quenched into ice water. After that this specimen was aged at 873–1073 K to form the γ'-$(Ni,Fe,Co)_3Ti$ phase precipitate in the γ phase. Microstructure observation was carried out by optical microscopy and field emission scanning electron microscopy (FE-SEM: JSM-7800F), and the hardness was evaluated by the microhardness test. The mechanical and SE properties were examined by the cyclic tensile test at a strain rate of 1.67×10^{-4} s^{-1} in a strain control mode using sheet specimens of 60 mm × 1 mm × 0.18 mm with mirror surface. Tensile strain was measured by monitoring the displacement of gauge length of 30 mm marked with two lines, by means of non-contact digital video extensometer. The martensitic transformation temperatures were determined in load-free condition by electrical resistivity (ER) measurement using the four-terminal method at a heating and cooling rate of 5×10^{-2} K s^{-1}. The determination of crystal structure of the precipitate on grain boundaries was carried out by powder X-ray diffractometry (XRD). The powder specimens of 0, 0.02, and 0.05 B with approximately 5 μm in diameter were prepared with a flat diamond file and aged at 973 K for 6 h after annealing at 1473 K for 5 min, followed by quenching to ice water. The crystalline orientation was examined by Electron Back-Scatter Diffraction (EBSD).

Results and Discussion

Microstructures and Vickers Hardness

Figure 1 shows the microstructures of (a) 0B, (b) 0.02B, and (c) 0.05B specimens aged at 973 K for 6 h and (d) 0.08B specimen as-solution treated at 1473 K. While the grain boundary precipitates are observed in the 0B specimen, the precipitation along grain boundaries is effectively suppressed in the 0.02B and 0.05B specimens. Especially, the contrast of grain boundary in the 0.05B specimen is the weakest of all. The grain boundary precipitates, however, were confirmed by SEM observation using back-scattering electron (BSE) with a higher magnification even in the 0.05B specimen, as shown in the inset of Fig. 1c. On the other hand, in the 0.08B alloy, the liquid phase already appears at the solution-treatment temperature of 1473 K, surrounding the γ matrix phase, caused by a decrease of solidus temperature.

In order to confirm the crystal structure of the grain boundary precipitates, powder samples underwent XRD measurement. Figure 2 shows the powder XRD patterns of the 0B, 0.02B, and 0.05B specimens aged at 973 K for 6 h. While for the 0.02B and 0.05B alloys, the low fraction of

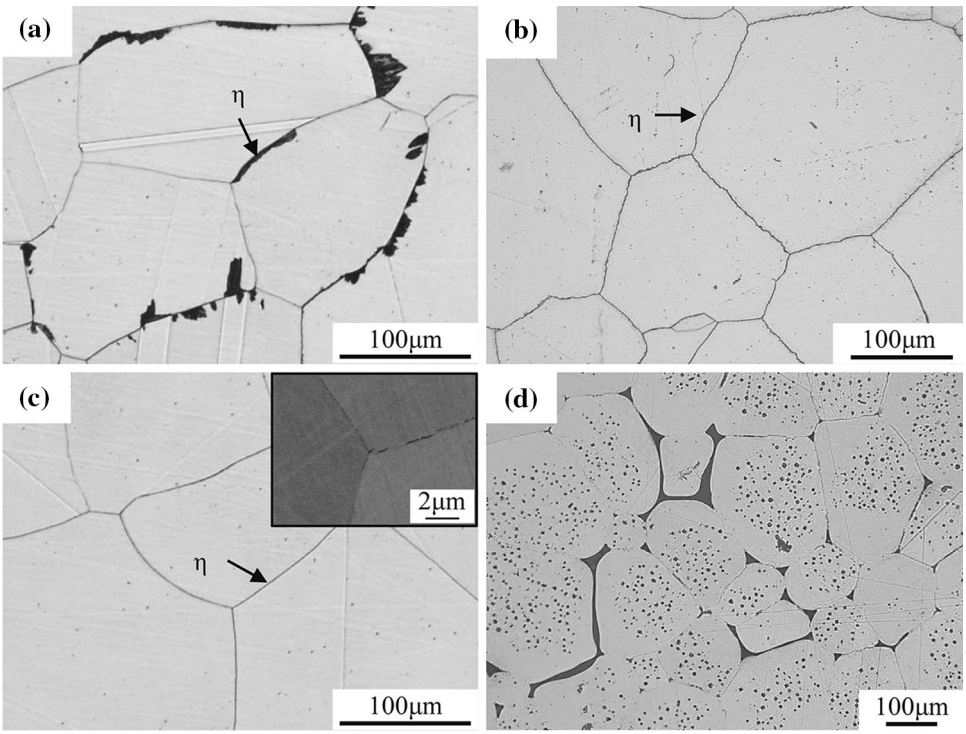

Fig. 1 Microstructures of **a** 0B, **b** 0.02B, and **c** 0.05B specimens aged at 973 K for 6 h and **d** 0.08B specimen solution-treated at 1473 K. *Inset* of **c**: BSE micrograph for 0.05B showing grain boundary precipitation

the grain boundary precipitate was not detected, the grain boundary phase of the 0 B specimen was confirmed as being the η-$D0_{24}$ phase, as reported by T. Maki et al. [6]. Thus, it is concluded that grain boundary precipitation is most effectively suppressed by the addition of 0.05 at. % boron as well as in the case of the Fe–Ni–Co–Al alloys [9, 16, 18, 20], without formation of the liquid phase at grain boundaries. It is well known that the grain boundary segregation of boron strengthens grain boundaries in Ni-based and Fe-based superalloys [30]. The segregated boron is considered to lower the grain boundary energy, resulting in suppression of precipitation in the present Fe–Ni–Co–Ti alloys.

It has been reported that a high level of hardness is required to obtain thermoelastic transformation in ferrous SMAs [1]. Vickers hardness of the 0, 0.02, and 0.05B alloys at 873, 973, and 1073 K is shown in Fig. 3. Vickers hardness of the alloy aged at 873 and 973 K monotonically increases with aging time as reported by Maki et al. [6], and aging at 973 K was found to most effectively enhance the hardness in contrast to aging at other temperatures. In a specimen aged at 1073 K, however, the hardness immediately increases and reaches maximum at 1 h and then gradually decreases. This behavior may be caused by loss of the lattice coherency between the γ and γ' phases, due to coarsening of γ' precipitates by over-aging. In Fig. 3, it is also seen that the Vickers hardness of all the samples aged at 873 and 973 K slightly increases with increasing B composition, which may be due to solution hardening.

Transformation Temperatures and Mechanical Properties

Figure 4 shows the ER curves for the 0B, 0.02B, and 0.05B alloy specimens after aging treatment at 973 K for 6 h, the hardness level being around 450 Hv as presented in Fig. 3. In all the samples, the martensitic transformation obviously appears and both the martensitic transformation starting temperature, M_s, and the reverse transformation finishing temperature, A_f, which are defined as shown in Fig. 4, increase by the addition of boron. Moreover, the thermal hysteresis given by $A_f - M_s$ also increases, reaching the largest value of about 34 K for the 0.05B alloy specimen. It is important to note that for the 0.02B and 0.05B alloys, the heating curve does not coincide with the cooling curve in the parent phase region, which means that some amount of the martensite phase remains in the temperature range above the A_f temperature. This is obviously related to the increase of the thermal hysteresis with increasing B content and may be caused by local stabilization for some amount of the martensite phase due to the introduction of dislocations. However, this result is apparently in discrepancy with the fact that the specimen with a higher content of B has a higher hardness, as shown in Fig. 3. The reason for this discrepancy is not clear.

Figure 5 shows the tensile stress–strain curves at 246 K of the 0B, 0.02B, and 0.05B alloy specimens aged at 973 K for 6 h after solution treatment, where the test temperature is higher than A_f temperature of each specimen. It can be

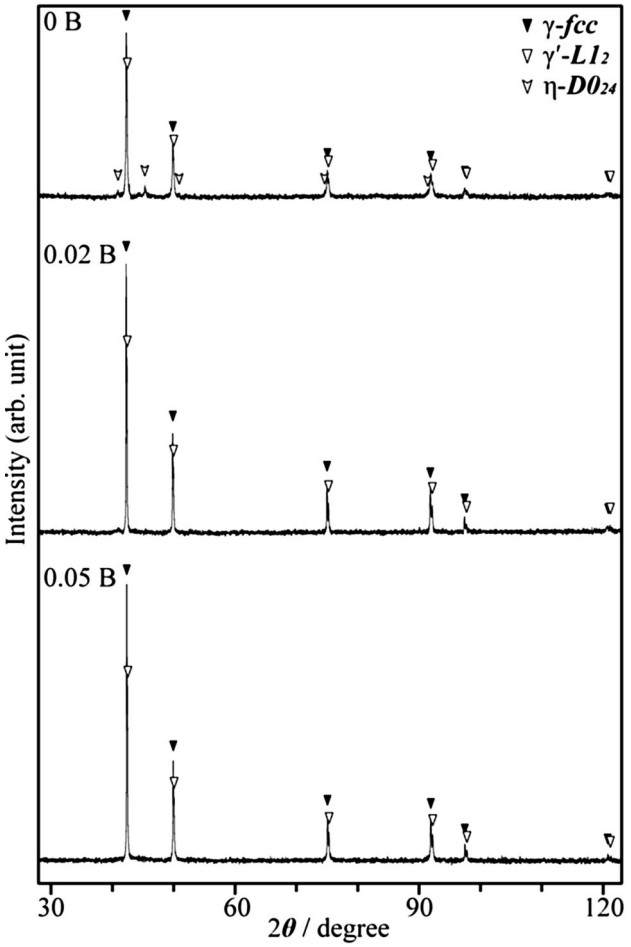

Fig. 2 Powder XRD patterns of the 0B, 0.02B, and 0.05B alloys aged at 973 K for 6 h

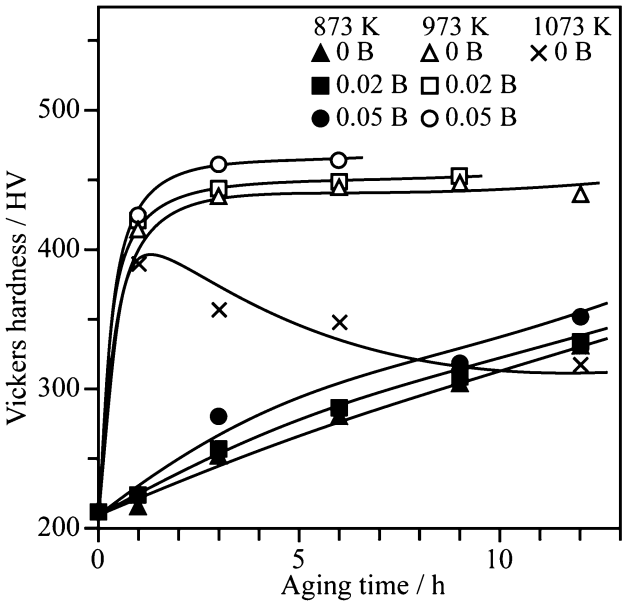

Fig. 3 Vickers hardness of 0, 0.02, and 0.05B alloys aged at 873, 973, and 1073 K for several lengths of time

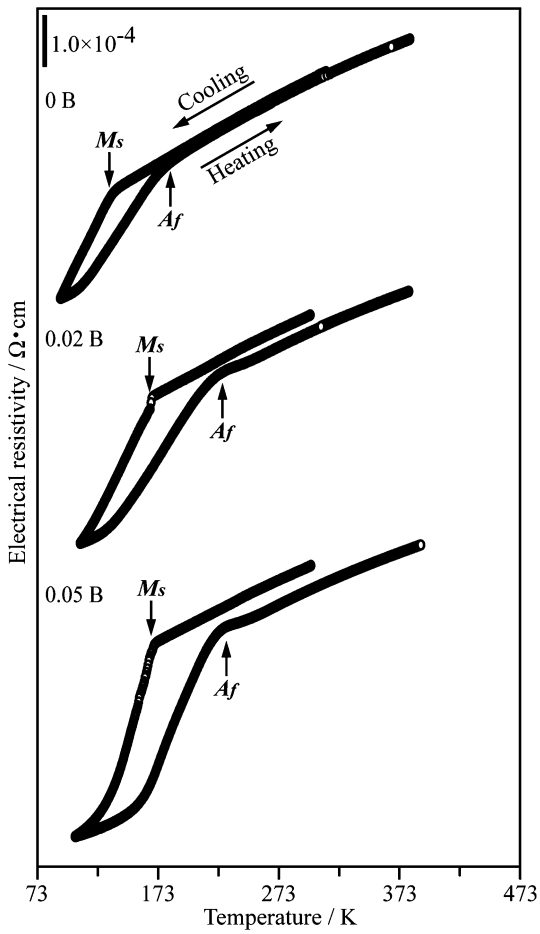

Fig. 4 Electrical resistivity curves during cooling and heating for 0B, 0.02B, and 0.05B specimens aged at 973 K for 6 h

seen that the 0.05B alloy specimen shows the highest elongation of about 1.3 % and the highest fracture stress of 784 MPa, whereas the elongation and the fracture stress in the other specimens are limited up to only 0.3 % and about 500–550 MPa, respectively. Since the degree of grain boundary precipitation in the 0.05B is clearly low, this result must be brought about by the increase of grain boundary strength due to suppression of the precipitation of the η phase at grain boundaries. The critical stress for stress-induced martensitic (SIM) transformation, σc, which is defined with 0.2 % proof stress, decreases with increase of the martensitic transformation temperatures by B addition. This fact suggests that the martensite was stress-induced in the tensile test. If being independent of B content in this alloy system, the temperature dependence of critical stress, $\partial\sigma c/\partial T$, can be estimated to be 3.0 MPa K^{-1} by the Clausius–Clapeyron relation with the differences in the *M*s temperature and the critical stress at 246 K of each specimen listed in Table 1. This value is almost the same as that

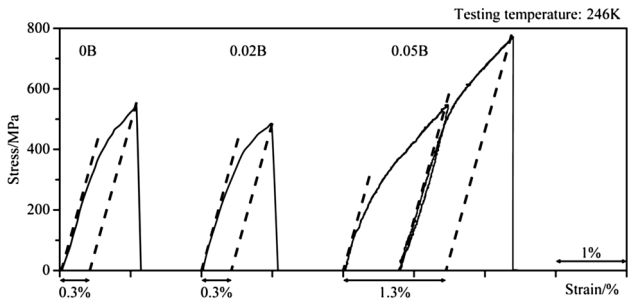

Fig. 5 Tensile stress–strain curves at 246 K for the 0B, 0.02B, and 0.05B alloy sheets aged at 973 K for 6 h after annealing at 1473 K for 3 h

Table 1 Summary of Ms temperature and critical stress for stress-induced martensitic transformation at 246 K of each specimen aged at 973 K for 6 h

	M_s temperature/K	Critical stress for transformation/MPa
0 B	135	465
0.02 B	168	420
0.05 B	172	315

in the Fe–Ni–Co–Al–Ta–B alloy [23] and about half of that in the Fe-28.9Ni-18.2Co-8.3Ti alloy [7].

Since the A_f of the 0.05B alloy is about 226 K, SE behavior can be expected in this test. An apparent SE behavior, however, could not be detected. Since the SIM transformation may occur as mentioned above, the steep slope of stress instead of a plateau suggests that the dislocations are introduced during the transformation. Therefore, no obvious SE behavior in the present alloy is probably caused by stabilization of martensite due to introduction of dislocations. In the case of Fe–Ni–Co–Al–Ta–B alloy fabricated with a similar thermomechanical treatment, dramatic improvements of both ductility and SE properties were realized by the strong {035}<100> texture, reaching about 20 and 13.5 %, respectively. In order to discuss the difference from the Fe–Ni–Co–Al–Ta–B alloy, the texture properties were examined by EBSD analysis.

Recrystallization Texture

Figure 6a, b shows the quasi-colored orientation maps and (100) pole figure in a 98.5 % cold-rolled sheet specimen of 0.05B alloy after solution treatment at 1473 K followed by quenching to ice water, respectively. Although a high reduction ratio of cold-rolling was carried out, the obtained recrystallization texture near {1 6 10}<4 1 1>, tilted by 18°–20° from {035}<100>, is not so strong, which may be insufficient to suppress grain boundary precipitation, as shown in Fig. 1c. Here, the fractions of low-angle and

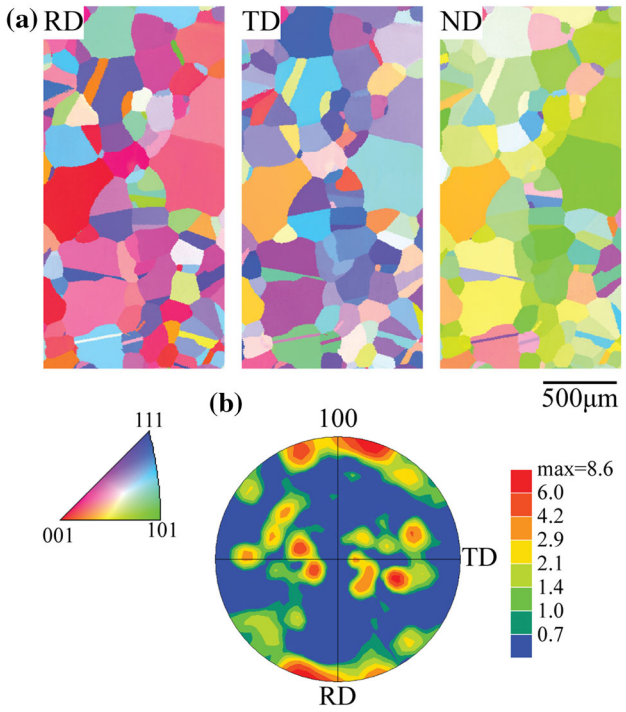

Fig. 6 **a** Quasi-colored orientation maps in RD, TD, and ND and **b** (100) pole figure taken from the sheet cold-rolled about 98.5 % after annealing at 1473 K for 3 h

coincidence site lattice boundaries were evaluated as being about 13 and 7 %, respectively, which are much lower than those (60 and 10 %, respectively) in the strongly textured Fe–Ni–Co–Al–Ta–B alloy [9]. It is known that grain boundary precipitation, which makes the grain boundaries brittle, can be suppressed by increasing the fraction of the low-energy boundaries such as low-angle and coincidence site lattice boundaries [31]. The lower level of the fracture strain in the present alloy obviously results from the high fraction of the high-energy random boundaries.

It is also known that the SE properties are influenced by strength and crystalline orientation [9]. The absence of SE strain in the present alloy may be brought about by the weak texture. On the other hand, Kokorin et al. have reported a faint SE strain at 240 K by bending test using the hot-forged Fe-28.9Ni-18.2Co-8.3Ti alloy sheet [7], where the texture seems to be weak. Their alloy has a composition different from that in the present alloy, including higher contents of Co and Ti. Because the obviously result in the increase of volume fraction of the γ' precipitates, the higher Co and Ti contents must make the alloy harder than in the case of the present alloy and improve the SE properties. Further systematic investigations for alloys with different Co and Ti contents are required to obtain improvement in SE and mechanical properties of the Fe–Ni–Co–Ti–B alloy.

Summary

For Fe-31.9Ni-9.6Co-4.7Ti alloys, the effects of the addition of B and thermomechanical treatment on microstructure and mechanical properties were investigated and the following results were obtained:

1. The grain boundary precipitation of the η phase during aging treatment obviously decreases with increasing B composition, being successfully restrained especially in the 0.05 at.% B alloy, while not being perfectly suppressed.
2. Vickers hardness monotonically increases with aging time in the alloys aged at 873 and 973 K, whereas it suddenly increases initially and then gradually decreases in that aged at 1073 K. Vickers hardness slightly rises with increasing B composition, reaching approximately 450 Hv by aging at 973 K.
3. Martensitic transformation temperatures and thermal hysteresis in the alloys aged at 973 K for 6 h gradually increase by the addition of B. For the 0.02B and 0.05B alloys, the heating curve does not coincide with the cooling one in the parent phase region. This suggests a partial stabilization of the martensite phase.
4. The tensile fracture elongation and fracture stress of the 0.05B alloy sheet aged at 973 K for 6 h are 1.3 % and 784 MPa, respectively, and no SE property could be detected in the tensile stress–strain curve. This may be caused by lack in hardness and texture in the alloy sheets with low contents of Co and Ti. Temperature dependence of critical stress in present alloy is estimated as being 3.0 MPa K^{-1}.

Acknowledgments This study was supported by a Grant-in-Aid from the Japanese Society for the Promotion of Science (JSPS) and by a Grant for Excellent Graduate Schools, Tohoku University, MEXT, Japan.

References

1. Otsuka K, Wayman CM (eds) (1998) Shape memory materials. Cambridge University Press
2. Sato A, Chishima E, Soma K, Mori T (1982) Shape memory effect in γ ⇄ ε transformation in Fe-30Mn-1Si alloy single crystals. Acta Metall 30:1177–1183
3. Kajiwara S, Liu D, Kikuchi T, Shinya N (2001) Remarkable improvement of shape memory effect in Fe–Mn–Si based shape memory alloys by producing NbC precipitates. Scr Mater. 44:2809–2814
4. Kajiwara S, Kikuchi T (1990) Shape memory effect and related transformation behavior in Fe–Ni–C alloys. Acta Metall 38:847–855
5. Ganzula NN, Koval YN, Kokorin VV (1979) Tetragonality of the martensite lattice and characteristics of the gamma if and only if alpha transformation in decomposed substitutional solid solutions. Phys Met Metall 47(4):186–189
6. Maki T, Kobayashi K, Minato M, Tamura I (1984) Thermoelastic martensite in an ausaged Fe–Ni–Co–Ti alloy. Scr Metall 18:1105–1109
7. Kokorin VV, Samsonov YuI, Chernenko VA, Shevchenko OM (1989) Superelasticity in Fe-Ni-Co-Ti alloys. Phys Met Metall 67(5):202–204
8. Kakeshita T, Shimizu K, Maki T, Tamura I, Kijima S, Date M (1985) Magnetoelastic martensitic transformation in ausaged Fe–Ni–Co–Ti alloy. Scr Metall 19:973–976
9. Tanaka Y, Himuro Y, Kainuma R, Sutou Y, Omori T, Ishida K (2010) Ferrous polycrystalline shape memory alloy showing huge superelasticity. Science 327:1488–1490
10. Kireeva IV, Chumlyakov YI, Kirillov VA, Kretinina IV, Danil'son YN, Karaman I, Cesari E (2011) Thermoelastic γ-α′ martensitic transformations in FeNiCoAlTa aging single crystals. Russ Phys J 53:1103–1106
11. Evirgen A, Ma J, Karaman I, Luo ZP, Chumlyakov YI (2012) Effect of aging on the superelastic response of a single crystalline FeNiCoAlTa shape memory alloy. Scr Mater. 67:475–478
12. Ma J, Hornbuckle BC, Karaman I, Thompson GB, Luo ZP, Chumlyakov YI (2013) The effect of nanoprecipitates on the superelastic properties of FeNiCoAlTa shape memory single crystals. Acta Mater 61:3445–3455
13. Krooß P, Holzweissig MJ, Niendorf T, Somsen C, Schaper M, Chumlyakov YI, Maier HJ (2014) Thermal cycling behavior of an aged FeNiCoAlTa single-crystal shape memory alloy. Scr Mater. 81:28–31
14. Krooß P, Somsen C, Niendorf T, Schaper M, Karaman I, Chumlyakov Y, Eggeler G, Maier HJ (2014) Cyclic degradation mechanisms in aged FeNiCoAlTa shape memory single crystals. Acta Mater 79:126–137
15. Geng Y, Lee D, Xu X, Nagasako M, Jin M, Jin X, Omori T, Kainuma R (2015) Coherency of ordered γ′ precipitates and thermoelastic martensitic transformation in FeNiCoAlTaB alloys. J Alloy Compd 628:287–292
16. Omori T, Abe S, Tanaka Y, Lee DY, Ishida K, Kainuma R (2013) Thermoelastic martensitic transformation and superelasticity in Fe–Ni–Co–Al–Nb–B polycrystalline alloy. Scr Mater. 69:812–815
17. Chumlyakov YuI, Kireeva IV, Poklonov VV, Pobedennaya ZV, Karama I (2014) The shape-memory effect and superelasticity in single-crystal ferromagnetic alloy FeNiCoAlTi. Tech Phys Lett 40:17 **(in Russia)**
18. Lee D, Omori T, Kainuma R (2014) Ductility enhancement and superelasticity in Fe-Ni-Co-Al-Ti-B polycrystalline alloy. J Alloy Compd 617:120–123
19. Tseng LW, Ma J, Karaman I, Wang SJ, Chumlyakov YI (2015) Superelastic response of the FeNiCoAlTi single crystals under tension and compression. Scr Mater. 101:1–4
20. Tanaka Y, Kainuma R, Omori T, Ishida K (2015) Alloy design for Fe–Ni–Co–Al-based superelastic alloy. Mater Today 2S:S485–S492
21. Omori T, Watanabe K, Umetsu RY, Kainuma R, Ishida K (2009) Martensitic transformation and magnetic field-induced strain in Fe–Mn–Ga shape memory alloy. Appl Phys Lett 95:082508
22. Zhu W, Liu EK, Feng L, Tang XD, Chen JL, Wu GH, Liu HY, Meng FB, Luo HZ (2009) Magnetic-field-induced transformation in FeMnGa alloys. Appl Phys Lett 95:222512
23. Omori T, Ando K, Okano M, Xu X, Tanaka Y, Ohnuma I, Kainuma R, Ishida K (2011) Superelastic effect in polycrystalline ferrous alloys. Science 333:69–71
24. Omori T, Nagasako M, Okano M, Endo K, Kainuma R (2012) Microstructure and martensitic transformation in Fe–Mn–Al–Ni shape memory alloy with B2-type coherent fine particles. Appl Phys Lett 101:231907
25. Omori T, Okano M, Kainuma R (2013) Effect of grain size on superelasticity in Fe–Mn–Al–Ni shape memory alloy wire. APL Mater. 1:032103

26. Tseng LW, Ma J, Wang SJ, Karaman I, Kaya M, Luo ZP, Chumlykov YI (2015) Superelastic response of a single crystalline FeMnAlNi shape memory alloy under tension and compression. Acta Mater 89:374–383
27. Vollmer M, Segel C, Krooß P, Günther J, Karaman I, Weidner A, Biermann H, Niendorf T (2015) On the effect of gamma phase formation on the pseudoelastic performance of polycrystalline Fe–Mn–Al–Ni shape memory alloys. Scr Mater. 108:23–26
28. Tseng LW, Ma J, Hornbuckle BC, Karaman I, Thompson GB, Luo ZP, Chumlyakov YI (2015) The effect of precipitates on the superelastic response of [100] oriented FeMnAlNi single crystals under compression. Acta Mater 97:234–244
29. Jia CC, Ishida K, Nishizawa T (1994) Partition of alloying elements between $\gamma(A1)$, $\gamma'(L1_2)$, and $\beta(B2)$ phases in Ni–Al base systems. Metall Mater Trans A 25:473
30. Sims CT, Stoloff NS, Hagel WC (eds) (1987) Superalloys II. Willy, New York
31. Watanabe T, Fujii H, Oikawa H, Arai KI (1989) Grain boundaries in rapidly solidified and annealed Fe-6.5 mass% Si polycrystalline ribbons with high ductility. Acta Metall 37:941–952